ACS APPLIED MATERIALS & INTERFACES

Article

Scalable Production of Sensor Arrays based on High Mobility Hybrid Graphene Field Effect Transistors

Zhaoli Gao, Hojin Kang, Carl H. Naylor, Frank Streller, Pedro Ducos, Madeline D. Serrano, Jinglei Ping, Jonathan Zauberman, Rajesh Rajesh, Robert W Carpick, Ying-Jun Wang, Yung Woo Park, Zhengtang Luo, Li Ren, and A.T. Charlie Johnson

ACS Appl. Mater. Interfaces, **Just Accepted Manuscript** • DOI: 10.1021/acsami.6b09238 • Publication Date (Web): 27 Sep 2016

Just Accepted

ACS Publications

ACS Applied Materials & Interfaces is published by the American Chemical Society. 1155 Sixteenth Street N.W., Washington, DC 20036

Scalable Production of Sensor Arrays based on High Mobility Hybrid Graphene Field Effect Transistors

Zhaoli Gao[1,2,†], Hojin Kang[1,3,†], Carl H. Naylor[1], Frank Streller[4], Pedro Ducos[1], Madeline D. Serrano[1], Jinglei Ping [1], Jonathan Zauberman[1], Rajesh[5], Robert W. Carpick[4], Ying-Jun Wang[6], Yung Woo Park[3], Zhengtang Luo[2], Li Ren[6,], A.T. Charlie Johnson[1,*]*

[1]Department of Physics and Astronomy, University of Pennsylvania, Philadelphia, 19104, USA

[2]Department of Chemical and Biomolecular Engineering, Hong Kong University of Science and Technology, Clear Water Bay, Kowloon, Hong Kong

[3]Department of Physics and Astronomy, Seoul National University, Seoul 151-747, Republic of Korea

[4]Department of Materials Science and Engineering, University of Pennsylvania, Philadelphia, 19104, USA

[5]CSIR-National Physical Laboratory, Dr. K. S. Krishnan Road, new Delhi-110012, India

[6]School of Materials Science and Engineering, South China University of Technology, Guangzhou 510006, PR China

Correspondence to: cjohnson@physics.upenn.edu and psliren@scut.edu.cn.

†Zhaoli Gao and Hojin Kang contributed equally to this work.

Keywords: graphene, gold nanoparticles, scalable fabrication, bilayer photolithography process, DNA biosensor,

Abstract

We have developed a scalable fabrication process for production of DNA biosensors based on gold nanoparticle-decorated graphene field effect transistors (AuNP-Gr-FETs), where monodisperse AuNPs are created through physical vapor deposition followed by thermal annealing. The FETs are created in a four-probe configuration, using an optimized bilayer photolithography process that yields chemically clean devices, as confirmed by XPS and AFM, with high carrier mobility (3590 ± 710 cm^2/V-s) and low unintended doping (Dirac voltages of 9.4 ± 2.7 V). The AuNP-Gr-FETs were readily functionalized with thiolated probe DNA to yield DNA biosensors with a detection limit of 1 nM and high specificity against non-complementary DNA. Our work provides a pathway toward the scalable fabrication of high-performance AuNP-Gr-FET devices for label-free nucleic acid testing in a realistic clinical setting.

Introduction

Noble metal nanoparticle-graphene (NP-Gr) hybrid structures hold tremendous promise for label-free biosensing applications,[1-7] in which graphene functions as an ideal transducer due to its 2D nature, biocompatibility,[8] and high carrier mobility.[9] In contrast to linker molecules such as pyrene,[10-11] diazonium[12] and BSA-streptavidin,[13] noble metal NPs allow simple, fast and efficient immobilization of the functionalized receptor molecules on the biosensors through covalent bonds, such as Au-S[4] and Pt-S.[5] These properties make NP-Gr field effect transistors (FETs) suitable for label-free clinical diagnosis and genomics, such as DNA biosensors for molecular diagnostics.[14] Nucleic acid testing is of particular interest since it

may enable diagnosis of a bacterial or viral infection during the window period when a patient is already infected but will not yet show up as positive by an antibody test.

So far most attempts have been devoted to biosensors based on reduced graphene oxide (rGO) for the detection of proteins,[1] microRNA,[6] and DNA oligomers.[5] Encouraging progress has been achieved, including nM-level detection of target DNA in real-time.[5] Despite the ease of preparation for rGO, it is difficult to control the rGO thickness, uniformity and channel dimensions.[15] Consequently, device performance is frequently degraded compared to graphene-based devices, with relatively low carrier mobility (<10 cm^2/V-s),[16] on-off ratio (< 2)[17] and yield. Dong *et al.*[4] reported on a DNA biosensor based on chemical vapor deposited (CVD) graphene) decorated with gold NPs. However, their process was focused on single device preparation and they did not report on process reproducibility, control of graphene channel dimensions, and electrical performance such as carrier mobility. There is as yet no report on a scalable, reproducible, and high quality fabrication process of NP-Gr hybrid FETs, which is a critical step towards practical biosensor applications.

In this work, we demonstrated a novel, wafer-scale fabrication process for arrays of DNA biosensors based on gold nanoparticle-decorated graphene field effect transistors (AuNP-Gr-FET) measured in a four-probe configuration. The devices were of high quality, with hole mobilities of 3590 ± 710 cm^2/V-s and Dirac voltages of 9.4 ± 2.7 V. This approach thus offers significant performance advantages over the NP-rGO materials discussed above, i.e., mass production capability (full wafer fabrication of 9 chips, each contains 24 devices), high reproducibility (> 90% yield), high carrier mobility and low unintended doping level. The high quality is attributed in part to the use of a photolithography process that includes a polydimethylglutarimide (PMGI) protective layer,[18] which largely eliminates photoresist

residues on the graphene channel, as confirmed by AFM, XPS, and electrical measurements. Physical deposition of a sub-monolayer of gold followed by thermal annealing was used to decorate the graphene with AuNPs with a high density (~ 400/μm^2) and relatively tight diameter distribution (5.3 ± 1.2 nm), enabling dense functionalization with thiolated probe single-stranded DNA oligomers. After exposure to target DNA, a positive Dirac voltage shift is observed whose magnitude varies with target concentration, in agreement with an electrostatic gating mechanism.[12] A detection limit of 1 nM was achieved, with good specificity against non-complementary ssDNA oligomers. Since reliable and reproducible sensing results are important for detection of biomolecules, this work provides a clear route to a scalable fabrication process for large arrays of high-performance AuNP-Gr-FET devices, with potential applications for label-free DNA biosensors and immunoassays.

Materials and Methods

Graphene synthesis and Au deposition: Graphene synthesis was carried out by low-pressure chemical vapor deposition (OTF-1200X-4-C4-SL-UL, MTI Corp.). Cu foils (Alfa Aesar Item #46365) were cleaned with 5.4% HNO_3 for 40 seconds and two DI water baths for 2 min, and then blown dry with N_2 gas. The reaction chamber was pumped to a base pressure of ~ 0.05 Torr. The Cu growth substrate was annealed at 1020 °C for 30 minutes with a gas flow of 500 sccm Ar and 80 sccm H_2. Monolayer graphene was then grown using methane as a carbon source at a flow rate of 5 sccm for 5 mins and then 10 sccm for 15 mins. The reactor was subsequently cooled to room temperature rapidly under a flow of 80 sccm H_2 and 10 sccm CH_4. A submonolayer of gold was then deposited onto the graphene by thermal evaporation to a nominal thickness of 2 Å at a rate of 0.15 Å/s, as determined by a quartz crystal microbalance monitor.

AuNP-Gr-FET sensor array fabrication: Standard photolithographic processing was used to define an electrode array for 24, four-probed graphene FETs on a highly p-doped Si wafer with a 300 nm thermal oxide layer. The contact metallization was 5 nm Cr / 40 nm Au, deposited by thermal evaporation. To minimize doping of the graphene FETs by substrate defects,[19] the electrode array was treated with HMDS to yield a hydrophobic surface. Graphene covered by a gold submonolayer was transferred onto the metallized SiO_2/Si chip using the PMMA assisted "bubbling" transfer method.[2, 16] Briefly, PMMA coated Au/graphene/Cu was slowly immersed into a 0.05 M NaOH solution with a 20 V potential difference applied between the copper foil and the solution. PMMA supported Au/graphene was separated from the Cu foil by gas bubbles formed at the Cu surface. After three DI water baths, the PMMA/graphene film was transferred onto the metallized SiO_2/Si chip with the gold layer oriented away from the substrate, followed by air drying and baking at 150 ˚C for 3 minutes to enhance adhesion between the graphene and the substrate. After removal of PMMA with acetone, the chips were spin coated with a photoresist bilayer of PMGI (MicroChem Corp.) and S1813 (Shipley). Graphene channels were defined using by photolithography and oxygen plasma etching (Pressure: 1.25 Torr, Power: 50 W, Duration: 35 seconds). The photoresist residue on graphene channels was removed by a N-Methyl Pyrrolidinone (NMP) based stripper (NANO^{TM} Remover PG , MicroChem Corp.), acetone and IPA to obtain the array of 24 FETs. Finally, the array was annealed in H_2/Ar forming gas at 225 ˚C to reduce photoresist residues and to allow the formation of relatively monodisperse AuNPs through a nucleation and growth process in which the free energy of Au clusters is minimized.[20]

SEM, AFM and XPS Characterization: The morphology of the AuNPs was characterized by field-emission scanning electron microscopy (SEM, JEOL, 7500F) with an acceleration voltage of 18 kV. An atomic force microscope (AFM, Icon Bruker) equipped with a probe

with a tip radius of <10 nm (TAP300Al-G, Budgetsensors) was used to characterize the topography of the AuNPs. The graphene surface was investigated by XPS using a customized XPS spectrometer (VG Scienta AB, Uppsala, Sweden).[21] XPS analyses were performed using a monochromatic Al Kα source (photon energy:1486.6 eV). The residual pressure in the analysis chamber was maintained at less than 10^{-8} Torr. The spectrometer was calibrated according to ISO 15472:2001 with an accuracy of ± 0.05 eV. Survey and high-resolution spectra were acquired in constant-analyzer-energy mode with pass energies of 200 and 100 eV, respectively. The spectra were processed using CasaXPS software (v.2.3.16, Casa Software Ltd., Wilmslow, Cheshire, U.K.). Background subtraction was performed using the Shirley−Sherwood method. The quantitative evaluation of XPS data was based on integrated intensity using a first-principles model and applying Powell's equation.[22]

Functionalization with probe DNA and testing against target or control solutions: Arrays of AuNP-Gr-FET sensors were incubated in 1 μM aqueous solution of thiolated probe DNA with a T_{10} spacer between the recognition sequence and the thiol functional group[23] ((SH)-TTTTTTTTTTAGCCGGGCGAGATACCCAATGCGC (5' to 3')) in DI water for 1 hour in a humid atmosphere to suppress the evaporation of the DNA solution. The array was then treated with 0.1% Tween 20 aqueous solution for 1 hour to remove probe DNA adsorbed nonspecifically on the graphene and to act as a blocker against non-specific binding of target DNA. This was followed by washing with two 0.05% Tween 20 solution baths and one DI water bath (2 min each) and drying with N_2 gas. After FET measurement, the probe DNA-immobilized AuNP-Gr-FET devices were immersed in 12 mL of complementary target DNA (cDNA) (GCGCATTGGGTATCTCGCCCGGCT (5' to 3')) or a control solution of non-complementary DNA (non-cDNA) (CTTCTGTCTTGATGTTTGTCAAAC (5' to 3')) of different concentrations in 0.1 % Tween 20 solution for 2.5 hours to allow for DNA

hybridization. The devices were washed with two 0.05% Tween 20 solution baths and one DI water bath, followed by drying with N_2 gas before measurement of the electrical properties.

Electrical measurement and evaluation: Electrical measurements were performed under ambient conditions in a probe station equipped with a probe card that is capable of measuring the 24 devices simultaneously. Conductivity-gate voltage (σ-V_g) measurements were carried out using a Keithley 2400 sourcemeter, with a bias current of 10 μA, with a four-probe geometry (Fig. 1c) to eliminate the effect of the contact resistance or Schottky barriers formed at the graphene-electrode interface[24]. The gate voltage was applied using a Keithley 6487 voltage source. Dirac point voltage and hole carrier mobility were extracted by fitting the hole branch of the σ-V_g curve to the equation[25-27]:

$$\sigma^{-1}(V_g) = [\mu c_g (V_D - V_g)]^{-1} + {\sigma_s}^{-1} \quad (1)$$

where c_g is the gate capacitance per unit area for the 300nm thick SiO_2 (11.5 nF/cm^2), μ is the hole carrier mobility, V_D is the Dirac voltage, and σ_s is the saturation conductivity as $V_g \to -\infty$.

Results and Discussion

Figure 1a shows a schematic of the sensor array fabrication process; details are provided in the Methods section. The process is designed for fabrication of nine arrays, each consisting of 24 devices in a four-probe configuration, on a 4-inch wafer (Fig. 1b-d). Large-area monolayer graphene films (10 cm × 15cm) were synthesized on Cu foil by low-pressure chemical vapor deposition (CVD). Following graphene growth, a (nominally) 2 Å-thick submonolayer of gold was thermally deposited onto the CVD graphene. Using the PMMA assisted bubbling method, the Au/graphene was transferred onto a 300 nm thick SiO_2 substrate with pre-fabricated Cr/Au electrodes for an array of 24 four-probed graphene FETs. FET channel

regions were then defined in the Au-graphene layer using a bilayer photolithography process and oxygen plasma etching. After removal of residual photoresist with Remover PG and wafer dicing, the FET array was annealed in an H_2/Ar atmosphere at 225 ˚C for 1 hour, which both removes photoresist residues and encourages the growth of relatively monodisperse AuNPs on the surface of the device.[20]

The fabrication process included the use of a resist bilayer (PMGI protective layer and S1813 imaging layer) in order to reduce photoresist residues on the graphene and thereby improve the performance of the FETs. The effectiveness of this approach was assessed by AFM, XPS, and electrical characterization of graphene FETs without AuNP decoration. When the photolithography process included only S1813, considerable contamination was observed by AFM (Fig. 2a, lower panel), while no evidence of a scum layer was found for a similar sample processed using the bilayer process (Fig. 2a, upper panel). To confirm the chemical identity of the residue, a quantitative XPS analysis of the graphene surface was performed before and after photolithographic processing. The overview XPS spectra (Fig. S1) show that the dominant elemental components (Si, C, O) were the same before and after photolithography. On a finer scale (Fig. S2), the C1s region of the spectrum (~ 282 – 292 eV) shows a main peak at 284.1 eV, associated with the sp^2 hybridized C-C bond of graphene, and three other peaks with chemical shifts of +1.3, +2.5, and +4.5 eV, which are assigned to C–OH, C=O and HO-C=O functional groups, respectively.[28]. Immediately after transfer, the relative integrated intensity of the satellite peaks compared to the main peak are 12.6 ± 1.8%, 5.8 ± 0.2%, and 3.0 ± 0.3%, which presumably reflects a very small amount of residue from the PMMA layer used during transfer. For the graphene FET array processed using a single layer of S1813 (Fig. 2c), the intensities increased dramatically, approximately doubling, to 22.6 ± 0.5%, 8.5 ± 0.8%, and 7.4 ± 0.4%, confirming the presence of significant

contamination. In contrast, the use of the bilayer resist scheme (Fig. 2d) leads to negligible increase in the satellite peaks (13.7 ± 0.6 %, 6.4 ± 0.4 %, and 2.0 ± 0.1 %); in fact, the peak associated with the HO-C=O functionality is reduced post processing. The XPS investigation thus confirms that PMGI acts as an effective protective layer in the photolithography process, resulting in a chemically cleaner surface for the graphene FET.

The electronic effect of the contamination was assessed using four-probed σ-V_g measurements of complete arrays of 24 graphene FETs processed using the two approaches (see Fig. 2b for typical FET σ-V_g curves). The σ-V_g curve for the FET fabricated using the bilayer process is very symmetric, and analysis of measurements of a full array show high hole carrier mobility of 3720 ± 170 cm^2/V-s and electron mobility of 3100 ± 450 cm^2/V-s and low doping as indicated by the Dirac voltage of 5.2 ± 0.5 V. In contrast, the σ-V_g curve for the FET processed using a single layer of S1813 is strongly asymmetric, with significantly lower mobility (hole: 1860 ± 250 cm^2/V-s, electron: 390 ± 290 cm^2/V-s) and greater doping (Dirac voltage of 11.6 ± 1.5 V). These observations are attributed to the fact that conventional imaging photoresists such as S1813 contain aromatic components that can bind strongly to the graphene surface through $\pi - \pi$ stacking interactions[18, 29] and degrade the electrical performance of graphene FETs. PMGI, which is free of novolac resin, can act as a protective layer for the graphene and reduce the photoresist residues. A similar method has previously been shown to effectively reduce the scum layer of photoresist residual on carbon nanotube FETs.[18] Our process therefore provides a strategy for cost-effective, large-scale fabrication of high-performance graphene FET arrays and compares very favorably with other reports of graphene FETs produced by photolithography, where the hole carrier mobility is typically lower than 2500 cm^2/V-s.[30-31]

AuNP-Gr-FETs were prepared using the photolithography bilayer process described above, with their surface morphology and electrical performance summarized in Figure 3. Scanning electron microscopy (SEM) shows that thermal deposition of 2Å of gold on to graphene led to the formation of small gold clusters on the surface (Fig. S3a). After definition of the FET channels, these gold clusters were transformed by annealing into nanoparticles with a uniform number density of ~ 400/μm^2 (Fig. S3c). AFM topographic images (Fig. 3a) and corresponding analysis of the nanoparticle heights (Fig. 3b) shows an approximately Gaussian diameter distribution centered at 5.3 ± 1.2 nm. The Raman spectrum of the AuNP-Gr hybrid layer reveals a 2D band located at 2689 cm^{-1}, which can be fit with a single Lorentzian with a full-width at half-maximum (FWHM) of 51 cm^{-1}, larger than that of the bare graphene (2D FWHM = 31 cm^{-1}, see Fig. S4), indicating that the graphene is doped by the AuNPs.[32] The Raman spectrum also shows a very small D band at ~1346 cm^{-1}, with I_D/I_G ratio of ~0.11, slightly larger than that of the pristine graphene (I_D/I_G ~ 0.07). This low I_D/I_G ratio suggests that the hybrid AuNP-Gr layer retains its high material quality.[30]

Four-probe σ-V_g measurements conducted on arrays of AuNP-Gr devices confirm the high material quality (see Fig. S5 for a representative curve). The devices have high hole mobility of 3590 ± 710 cm^2/V-s and electron mobility of 1670 ± 230 cm^2/V-s (Fig. 3c), only slightly less than the value found for undecorated GFET devices. Compared to earlier reports on AuNP-rGO FETs,[16] AuNP-Gr FETs show superior performance, with a mobility more than two orders of magnitude higher; indeed, the mobility values reported here are to our knowledge the highest to date for metal NP-Gr hybrid structures. The Dirac voltage of the AuNP-Gr-FET shows a positive shift to 9.4 ± 2.7 V (Fig. 3d) compared to devices without AuNPs (5.2 ± 0.5 V), corresponding to an induced dopant density of ~ 3.0×10^{11} cm^{-2} due to the AuNP decoration. This effect is ascribed to the work function difference between

graphene (~ 4.66 eV[33]) and gold (5.1 - 5.47 eV) which leads to p-doping of the graphene. The structural, optical and electrical measurements discussed above indicate that AuNP-Gr FET sensors are of high quality, with high carrier mobility and low unintended doping level.

To complete the fabrication of the DNA biosensor (see Fig. 4a for a schematic), the nanoparticles on the AuNP-Gr FET devices were functionalized with thiolated probe DNA by application of a 1μM solution in DI water. Devices were next treated with a solution of 0.1% Tween 20 in DI water in order to block exposed graphene areas that would enable undesirable non-specific binding of arbitrary DNA oligomers.[34-35] Tween 20 is a nonionic surfactant with good affinity for graphene that has been reported to deter non-specific binding of proteins on carbon nanotubes[36] and bacterial cells on rGO.[37] Tween 20 is also commonly used in PCR-ELISA to reduce non-specific binding of analyte DNA to enable detection of a specific PCR product. Four-probe σ-V_g measurements were conducted after each functionalization step. As shown in Fig. 4b, treatment with probe DNA led to a significant increase in the Dirac voltage (ΔV_D =59.6 ± 3.2 V), attributed to the chemical-gating effect[27] of probe-DNA molecules that become negatively charged due to ionization of phosphate groups in residual water. The (hole) carrier mobility of the AuNP-Gr FET was also reduced by ~70 % to 1100 ± 360 cm^2/V-s, presumably due to scattering associated with the bound, negatively charged DNA. Application of the Tween 20 blocker led to a negative shift of V_D by 16.0 ± 2.2 V and an increase in the carrier mobility to 1470 ± 60 cm^2/V-s, both consistent with the expectation that Tween 20 saturates the graphene surface and displaces nonspecifically bound probe DNA. Assuming chemical gating of 34 negative charges for each probe oligomer, the density of immobilized probe DNA is ~ 850 /μm^2, corresponding to about two probe DNA oligomers per AuNP.

Biosensor testing against target DNA was also carried out in 0.1% Tween, which allows specific binding of target oligomers with probe DNA to generate a sensor output but prevents undesirable non-specific binding of DNA on the graphene surface. Data documenting the effectiveness of this approach is presented in Table S1. To avoid cross-contamination, each array of biosensors was tested against a single concentration of complementary target DNA ("cDNA"). To avoid the possibility of time-dependent effects, care was taken to ensure that all samples were incubated for the same length of time. Figure 4b shows results from a typical experiment, where exposure to cDNA at a concentration of 100 nM in 0.1% Tween leads to a Dirac voltage shift of +13.6 ± 0.7 V. The sensor response for various concentrations of cDNA (Fig. 4c) is reported as ΔV_D^{rel}, the Dirac voltage shift relative to the shift measured upon exposure to 0.1% Tween in DI water (+ 7.7 V). The data are consistent with an electrostatic gating mechanism,[24, 38] where hybridization of target cDNA with probe DNA on the AuNP provides additional chemical gating of the graphene FET channel. The measurements agree well with a model based on the Langmuir isotherm describing the equilibrium binding of target cDNA to the probe:

$$\Delta V_D^{rel} = A \frac{c}{K_a + c} \qquad (2)$$

where A is the maximum response with all binding sites occupied, c is the cDNA concentration, and K_a represents the concentration at which half of the available binding sites are occupied. The best fit to the data yields values A = 8.2 ± 0.4 V; assuming chemical gating by 24 negative charges for each oligomer, the density of bound cDNA is ~ 250 μm^{-2}. Based on the probe DNA density inferred above, this implies a hybridization rate of ~30%, in good agreement with the expectation of 25-56% at room temperature .[39] The best fit value for K_a = 22.5 ± 9.4 nM, which is consistent with surface plasmon resonance experiments conducted by others.[40] In a control experiment, a biosensor array tested against 1μM (random sequence) non-cDNA had a Dirac voltage shift of 7.7 ± 1.0 V, essentially identical to the Dirac voltage

shift for pure buffer (0.1 % Tween in DI water), showing that the DNA biosensor has high specificity. The results suggest a limit of detection of approximately 1 nM (relative Dirac voltage shift of 1.3 ± 1 V) for this choice of cDNA. The 1 nM sensitivity we find is in the range of detection limits found in earlier reports on DNA sensing (pM to nM scale) [4-5, 13, 41], and our methodology allows scalable fabrication of the sensor arrays and device miniaturization (24 devices per array), making it potentially suitable for commercial production. It is also known that DNA biosensor sensitivity is affected by the length[41] and surface density[42] of the probe DNA, which suggest strategies to further improve the detection limit of the sensors.

Conclusions

In summary, a reproducible, high-quality fabrication process for large arrays of AuNP-Gr-FETs has been developed, where the devices are suitable for use as DNA biosensors. The fabrication approach incorporates chemical vapor deposited graphene with a submonolayer gold layer, an optimized photolithography process, and a four probe design for the Gr-FET channel, leading to AuNP-Gr-FETs with a hole mobility of 3590 ± 710 cm^2/V-s and a Dirac voltage of 9.4 ± 2.7 V. The photolithography step relies on the use of a PMGI layer that effectively avoids contamination of the graphene, as assessed by AFM and XPS. Annealing is used to form AuNPs on the graphene surface at a high density (~ 400/μm^2) with a tight diameter distribution (5.3 ± 1.2 nm). After attachment of probe DNA to the AuNPs, the devices act as DNA biosensors with high specificity against non-target DNA and a limit of detection of ~ 1 nM. The scalability and sensitivity of the AuNP-Gr-FET devices are potentially applicable for gene-expression investigations and label-free genetic diagnosis. The device structure should also be suitable for protein functionalization and immunoassay development.

Supporting Information

XPS spectra for the graphene samples before and after photolithography, XPS spectra of C 1s region for a transferred graphene sample before photolithographic processing, SEM images of graphene before and after annealing the submonolayer of Au, Raman spectra of graphene after photolithographic processing using bilayer PMGI/S1813 and AuNP-Gr hybrid layer after bubble transfer onto the SiO_2 substrate and thermal annealing, representative σ-V_g curve for a Au-Gr-FET device, I-V_g curve and histogram of Dirac voltage shift of Gr FET without AuNP and AuNP-Gr FET after immobilization with 100 uM probe DNA, summary of control DNA sensing experiments to show how the use of 0.1% Tween 20 suppresses non-specific binding of DNA.

Funding Sources

This work was supported by the National Science Foundation Accelerating Innovation in Research program AIR ENG1312202. R.L. acknowledges financial support from National Natural Science Foundation of China (51273072), the Science and Technology Innovation Council of Guangzhou, China (201508020123), and the Science and Technology Projects of Guangdong, China (2014B090907004). Z.L. appreciates supports from the Research Grant Council of Hong Kong SAR (Project number 16204815) and from Center for 1D/2D Quantum Materials and the Innovation and Technology Commission (ITC-CNERC14SC01).

References

(1) Mao, S.; Lu, G.; Yu, K.; Bo, Z.; Chen, J. Specific Protein Detection Using Thermally Reduced Graphene Oxide Sheet Decorated with Gold Nanoparticle-Antibody Conjugates. *Adv. Mater.* **2010,** *22*, 3521-3526.

(2) Abraham, S.; Nirala, N. R.; Pandey, S.; Srivastava, M.; Srivastava, S.; Walkenfort, B.; Srivastava, A. Functional Graphene-Gold Nanoparticle Hybrid System for Enhanced Electrochemical Biosensing of Free Cholesterol. *Anal. Methods* **2015,** *7*, 3993-4002.

(3) Turcheniuk, K.; Boukherroub, R.; Szunerits, S. Gold-Graphene Nanocomposites for Sensing and Biomedical Applications. *J. Mater. Chem. B* **2015,** *3*, 4301-4324.

(4) Dong, X.; Shi, Y.; Huang, W.; Chen, P.; Li, L.-J. Electrical Detection of DNA Hybridization with Single-Base Specificity Using Transistors Based on CVD-Grown Graphene Sheets. *Adv. Mater.* **2010,** *22*, 1649-1653.

(5) Yin, Z.; He, Q.; Huang, X.; Zhang, J.; Wu, S.; Chen, P.; Lu, G.; Zhang, Q.; Yan, Q.; Zhang, H. Real-Time DNA Detection Using Pt Nanoparticle-Decorated Reduced Graphene Oxide Field-Effect Transistors. *Nanoscale* **2012,** *4*, 293-297.

(6) Cai, B.; Huang, L.; Zhang, H.; Sun, Z.; Zhang, Z.; Zhang, G.-J. Gold Nanoparticles-Decorated Graphene Field-Effect Transistor Biosensor for Femtomolar Microrna Detection. *Biosens. Bioelectron.* **2015,** *74*, 329-334.

(7) Elshafey, R.; Siaj, M.; Tavares, A. C. Au Nanoparticle Decorated Graphene Nanosheets for Electrochemical Immunosensing of P53 Antibodies for Cancer Prognosis. *Analyst* **2016,** *141*, 2733-2740.

(8) Gurunathan, S.; Kim, J.-H. Synthesis, Toxicity, Biocompatibility, and Biomedical Applications of Graphene and Graphene-Related Materials. *Int. J. Nanomedicine* **2016,** *11*, 1927-1945.

(9) Banszerus, L.; Schmitz, M.; Engels, S.; Goldsche, M.; Watanabe, K.; Taniguchi, T.; Beschoten, B.; Stampfer, C. Ballistic Transport Exceeding 28 μm in CVD Grown Graphene. *Nano Lett.* **2016,** *16*, 1387-1391.

(10) Zhang, H.; Wang, Y.; Zhao, D.; Zeng, D.; Xia, J.; Aldalbahi, A.; Wang, C.; San, L.; Fan, C.; Zuo, X.; Mi, X. Universal Fluorescence Biosensor Platform Based on Graphene Quantum Dots and Pyrene-Functionalized Molecular Beacons for Detection of Micrornas. *ACS Appl. Mater. Interfaces* **2015,** *7*, 16152-16156.

(11) Cai, B.; Wang, S.; Huang, L.; Ning, Y.; Zhang, Z.; Zhang, G.-J. Ultrasensitive Label-Free Detection of PNA–DNA Hybridization by Reduced Graphene Oxide Field-Effect Transistor Biosensor. *ACS Nano* **2014,** *8*, 2632-2638.

(12) Lerner, M. B.; Matsunaga, F.; Han, G. H.; Hong, S. J.; Xi, J.; Crook, A.; Perez-Aguilar, J. M.; Park, Y. W.; Saven, J. G.; Liu, R.; Johnson, A. T. C. Scalable Production of Highly Sensitive Nanosensors Based on Graphene Functionalized with a Designed G Protein-Coupled Receptor. *Nano Lett.* **2014,** *14*, 2709-2714.

(13) Xu, G.; Abbott, J.; Qin, L.; Yeung, K. Y. M.; Song, Y.; Yoon, H.; Kong, J.; Ham, D. Electrophoretic and Field-Effect Graphene for All-Electrical DNA Array Technology. *Nat. Commun.* **2014,** *5*.

(14) Drummond, T. G.; Hill, M. G.; Barton, J. K. Electrochemical DNA Sensors. *Nat. Biotech.* **2003,** *21*, 1192-1199.

(15) Yin, P. T.; Shah, S.; Chhowalla, M.; Lee, K.-B. Design, Synthesis, and Characterization of Graphene–Nanoparticle Hybrid Materials for Bioapplications. *Chem. Rev.* **2015,** *115*, 2483-2531.

(16) Dong, X.; Huang, W.; Chen, P. In Situ Synthesis of Reduced Graphene Oxide and Gold Nanocomposites for Nanoelectronics and Biosensing. *Nanoscale Res. Lett.* **2010,** *6*, 1-6.

(17) Huang, X.; Yin, Z.; Wu, S.; Qi, X.; He, Q.; Zhang, Q.; Yan, Q.; Boey, F.; Zhang, H. Graphene-Based Materials: Synthesis, Characterization, Properties, and Applications. *Small* **2011,** *7*, 1876-1902.

(18) Khamis, S. M.; Jones, R. A.; Johnson, A. T. C. Optimized Photolithographic Fabrication Process for Carbon Nanotube Devices. *AIP Adv.* **2011,** *1*, 022106

(19) Lafkioti, M.; Krauss, B.; Lohmann, T.; Zschieschang, U.; Klauk, H.; Klitzing, K. v.; Smet, J. H. Graphene on a Hydrophobic Substrate: Doping Reduction and Hysteresis Suppression under Ambient Conditions. *Nano Lett.* **2010,** *10*, 1149-1153.

(20) Luo, Z.; Somers, L. A.; Dan, Y.; Ly, T.; Kybert, N. J.; Mele, E. J.; Johnson, A. T. C. Size-Selective Nanoparticle Growth on Few-Layer Graphene Films. *Nano Lett.* **2010,** *10*, 777-781.

(21) Mangolini, F.; Åhlund, J.; Wabiszewski, G. E.; Adiga, V. P.; Egberts, P.; Streller, F.; Backlund, K.; Karlsson, P. G.; Wannberg, B.; Carpick, R. W. Angle-Resolved Environmental X-Ray Photoelectron Spectroscopy: A New Laboratory Setup for Photoemission Studies at Pressures up to 0.4 Torr. *Rev. Sci. Instrum.* **2012,** *83*, 093112.

(22) Streller, F.; Agarwal, R.; Mangolini, F.; Carpick, R. W. Novel Metal Silicide Thin Films by Design Via Controlled Solid-State Diffusion. *Chem. Mater.* **2015,** *27*, 4247-4253.

(23) Hurst, S. J.; Lytton-Jean, A. K. R.; Mirkin, C. A. Maximizing DNA Loading on a Range of Gold Nanoparticle Sizes. *Anal. Chem.* **2006,** *78*, 8313-8318.
(24) Heller, I.; Janssens, A. M.; Männik, J.; Minot, E. D.; Lemay, S. G.; Dekker, C. Identifying the Mechanism of Biosensing with Carbon Nanotube Transistors. *Nano Lett.* **2008,** *8*, 591-595.
(25) Morozov, S. V.; Novoselov, K. S.; Katsnelson, M. I.; Schedin, F.; Elias, D. C.; Jaszczak, J. A.; Geim, A. K. Giant Intrinsic Carrier Mobilities in Graphene and Its Bilayer. *Phys. Rev. Lett.* **2008,** *100*, 016602.
(26) Chen, F.; Xia, J.; Ferry, D. K.; Tao, N. Dielectric Screening Enhanced Performance in Graphene FET. *Nano Lett.* **2009,** *9*, 2571-2574.
(27) Ping, J.; Xi, J.; Saven, J. G.; Liu, R.; Johnson, A. T. C. Quantifying the Effect of Ionic Screening on Protein-Decorated Graphene Transistors. *Biosens. Bioelectron.* **2015,** *in press*.
(28) Yumitori, S. Correlation of C1s Chemical State Intensities with the O1s Intensity in the XPS Analysis of Anodically Oxidized Glass-Like Carbon Samples. *J. Mater. Sci.* **2000,** *35*, 139-146.
(29) Tournus, F.; Charlier, J. C. Ab Initio Study of Benzene Adsorption on Carbon Nanotubes. *Phys. Rev. B, PRB* **2005,** *71*, 165421.
(30) Liang, X.; Sperling, B. A.; Calizo, I.; Cheng, G.; Hacker, C. A.; Zhang, Q.; Obeng, Y.; Yan, K.; Peng, H.; Li, Q.; Zhu, X.; Yuan, H.; Hight Walker, A. R.; Liu, Z.; Peng, L.-m.; Richter, C. A. Toward Clean and Crackless Transfer of Graphene. *ACS Nano* **2011,** *5*, 9144-9153.
(31) Shi, R.; Xu, H.; Chen, B.; Zhang, Z.; Peng, L.-M. Scalable Fabrication of Graphene Devices through Photolithography. *Appl. Phys. Lett.* **2013,** *102*, 113102.
(32) Wu, Y.; Jiang, W.; Ren, Y.; Cai, W.; Lee, W. H.; Li, H.; Piner, R. D.; Pope, C. W.; Hao, Y.; Ji, H.; Kang, J.; Ruoff, R. S. Tuning the Doping Type and Level of Graphene with Different Gold Configurations. *Small* **2012,** *8*, 3129-3136.
(33) Shan, B.; Cho, K. First Principles Study of Work Functions of Single Wall Carbon Nanotubes. *Phys. Rev. Lett.* **2005,** *94*, 236602.
(34) Johnson, R. R.; Johnson, A. T.; Klein, M. L. The Nature of DNA Base-Carbon Nanotube Interactions. *Small* **2010,** *6*, 31-34.
(35) Kybert, N. J.; Han, G. H.; Lerner, M. B.; Dattoli, E. N.; Esfandiar, A.; Johnson, A. T. C. Scalable Arrays of Chemical Vapor Sensors Based on DNA-Decorated Graphene. *Nano Research* **2014,** *7*, 95-103.
(36) Chen, R. J.; Bangsaruntip, S.; Drouvalakis, K. A.; Wong Shi Kam, N.; Shim, M.; Li, Y.; Kim, W.; Utz, P. J.; Dai, H. Noncovalent Functionalization of Carbon Nanotubes for Highly Specific Electronic Biosensors. *Proc. Natl. Acad. Sci. USA* **2003,** *100*, 4984-4989.
(37) Park, S.; Mohanty, N.; Suk, J. W.; Nagaraja, A.; An, J.; Piner, R. D.; Cai, W.; Dreyer, D. R.; Berry, V.; Ruoff, R. S. Biocompatible, Robust Free-Standing Paper Composed of a Tween/Graphene Composite. *Adv. Mater.* **2010,** *22*, 1736-1740.
(38) Lerner, M. B.; Resczenski, J. M.; Amin, A.; Johnson, R. R.; Goldsmith, J. I.; Johnson, A. T. C. Toward Quantifying the Electrostatic Transduction Mechanism in Carbon Nanotube Molecular Sensors. *J. Am. Chem. Soc.* **2012,** *134*, 14318-14321.
(39) Okahata, Y.; Kawase, M.; Niikura, K.; Ohtake, F.; Furusawa, H.; Ebara, Y. Kinetic Measurements of DNA Hybridization on an Oligonucleotide-Immobilized 27-MHz Quartz Crystal Microbalance. *Anal. Chem.* **1998,** *70*, 1288-1296.
(40) Nelson, B. P.; Grimsrud, T. E.; Liles, M. R.; Goodman, R. M.; Corn, R. M. Surface Plasmon Resonance Imaging Measurements of DNA and RNA Hybridization Adsorption onto DNA Microarrays. *Anal. Chem.* **2001,** *73*, 1-7.

(41) Ping, J.; Vishnubhotla, R.; Vrudhula, A.; Johnson, A. T. C. Scalable Production of High Sensitivity, Label-Free DNA Biosensors Based on Back-Gated Graphene Field Effect Transistors. *ACS Nano* **2016**.

(42) Duan, X.; Li, Y.; Rajan, N. K.; Routenberg, D. A.; Modis, Y.; Reed, M. A. Quantification of the Affinities and Kinetics of Protein Interactions Using Silicon Nanowire Biosensors. *Nat. Nano.* **2012,** *7*, 401-407.

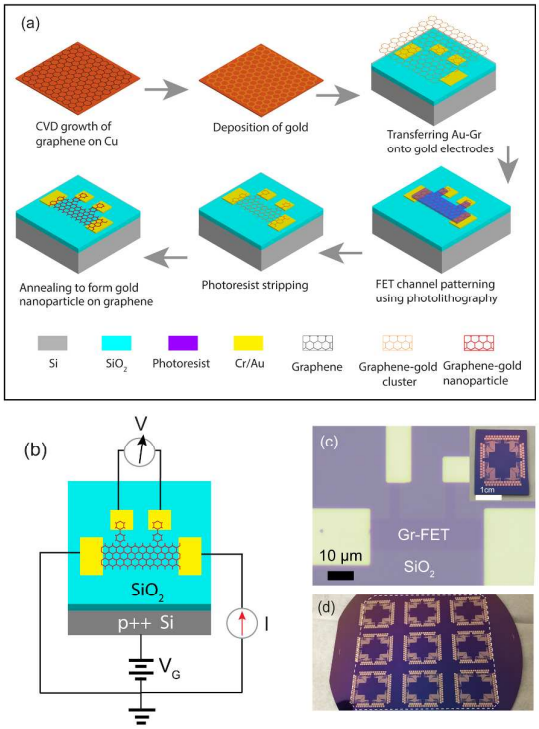

Figure 1. **Fabrication of AuNP-graphene FET arrays.** (a) Schematic showing the AuNp-Gr-FET fabrication process. A sub-monolayer gold film is deposited onto CVD grown graphene by thermal evaporation. The gold-graphene layer is coated with PMMA and transferred onto an electrode array on an Si/SiO_2 wafer. After removal of PMMA, FET channels are patterned using photolithography followed by oxygen plasma etching. Finally, the photoresist is removed, and the array is annealed to form AuNPs on the graphene. (b) Schematic of the four-probe conductivity-gate voltage measurement set up. (c) Optical micrograph showing an individual four-probed GFET device. Inset: Optical image of a chip with 24 Au-Gr-FET devices. Scale bar is 1 cm. (d) Optical image of a 4-inch wafer with 9 electrode arrays and a transferred graphene monolayer that covers the full region defined by the arrays (indicated by the dashed line).

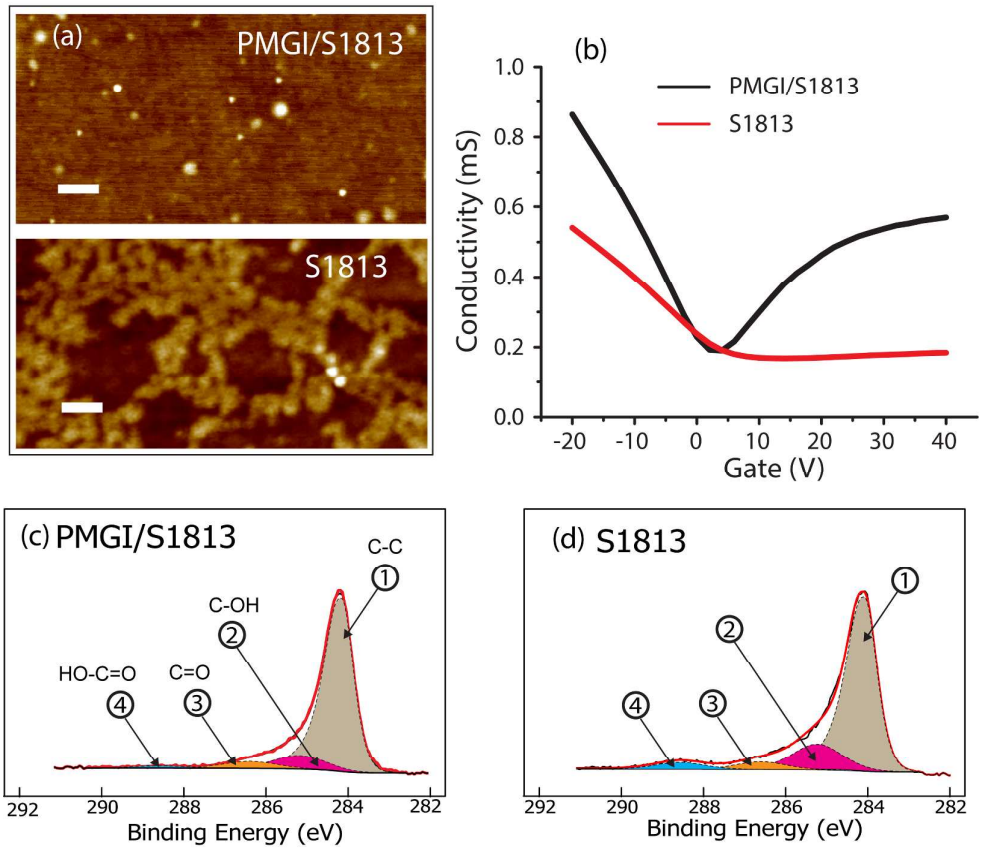

Figure 2. **Measurements of photoresist contamination on graphene after photolithographic processing.** (a) AFM images of the Gr-FET surface after photolithography and thermal annealing. The bilayer process results in low surface contamination (top image). In contrast, use of a single layer process leaves significant scum on the surface (bottom image). Scale bar is 100 nm. Vertical color scale is 5 nm. (b) σ-V_g curve of Gr-FETs fabricated using bilayer PMGI/S1813 (black data) and single layer S1813 (red data). Devices fabricated using the bilayer process are of higher quality with much higher carrier mobility and lower unintended doping. (c-d) XPS spectra of the C_{1s} regions for the samples processed using PMGI/S1813 (panel c) and S1813 (panel d). Both spectra are normalized to Peak 1, which is attributed to the the sp^2 hybridized C-C bond of graphene. The peaks labeled 2-4 are associated with C–OH, C=O and HO-C=O bonding in the contaminant layer. Peaks 2-4 are significantly reduced in the spectrum from the sample processed using PMGI/S1813, indicating a lower level of chemical contamination.

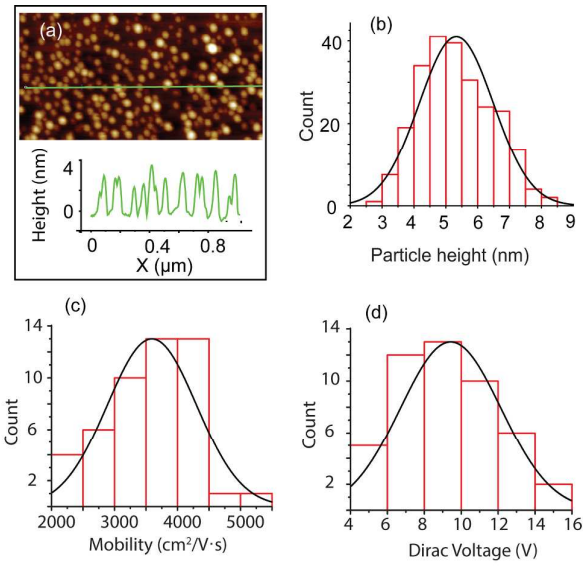

Figure 3. **AuNP-Gr FET structure and electrical properties.** (a) AFM image showing the formation of uniform AuNPs on graphene after annealing. The corresponding AFM line scan is shown below the AFM image. (b) AuNP size distribution. The AuNP diameter is 5.3 ± 1.2 nm. Histograms of (c) hole mobility and (d) Dirac voltage with Gaussian fits (black curve) of AuNP-Gr-FETs based on three separate arrays, with 24 devices each.

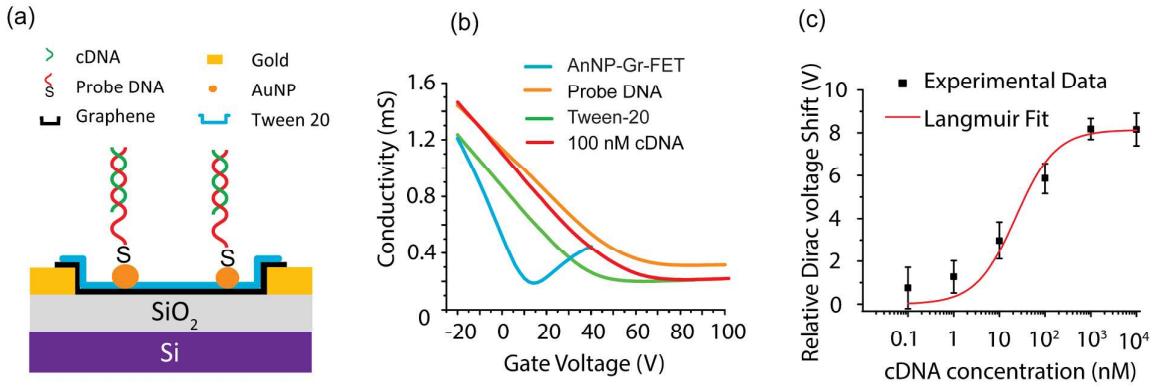

Figure 4. **Biosensor schematic and performance.** (a) Schematic of the AuNP-Gr-FET DNA biosensor. (b) σ-V_g curves after chemical functionalization and expsoure to target cDNA. After functionalization with probe DNA and Tween-20 blocker, exposure to 100 nM cDNA leads to a Dirac voltage shift of 13.6 V (green curve to red curve). (c) Sensor response as a function of cDNA concentration. Error bars are standard deviation of the mean. The red curve is a fit to a model based on the Langmuir isotherm. The limit of detection is ~1 nM.

Table of Contents Graphic